UNIVERSITY OF SOUTHAMPTON

INSTITUTE OF SOUND AND VIBRATION RESEARCH

FLUID DYNAMICS AND ACOUSTICS GROUP

The Cavitation Of Bubbles Containing Mon-, Di-, And Tri-Atomic Gases: Discussion Through Modelling Of Dynamics Using The Gilmore Equation

by

T.G. Leighton and A.D. Phelps

ISVR Technical Report No. 248

September 1995

Approved: Group Chairman, Professor C. L. Morfey

ACKNOWLEDGEMENTS

T.G. Leighton wishes to thank the British Council in Japan for assisting with the travel expenses which made collaboration with Dr Kondo possible.

ABSTRACT

The cavitation dynamics of single gas bubbles in water in a 1 MHz sound field of acoustic pressure amplitude 0.424 MPa are modelled for the first fifty cycles using the Gilmore equation. The bubble may contain either helium, oxygen, or carbon dioxide, illustrating the behaviours of mon-, dia- and tri-atomic gases respectively. The surrounding water is taken to be saturated with the dissolved gas, and mass flux across the bubble wall is incorporated into the model. The resulting temperatures attained during the collapses are used to interpret a scheme of experimental observations.

CONTENTS

List of Tables	(v)
List of Figures	(vi)
Introduction	1
Methods	2
Results	3
Discussion	3
Conclusions	5
References	6
Tables	8
Figures	9

LIST OF TABLES

Page

8 ***Table 1:*** Summary of the experimental findings of Kondo and co-workers (Kondo 1994, personal communication). The symbol '+' indicates a positive finding, the more symbols the greater the magnitude of the effect observed. The symbol '-' indicates that the effect was not observed. The symbol '+/-' indicates a marginal effect.

8 ***Table 2:*** Data for calculations employed in the Gilmore model, and for other relevant gases.

LIST OF FIGURES

Page

9 ***Figure 1*:** Modelling results on a Helium filled bubble incorporating mass flux across the bubble wall. The bubble is initially at rest in water at 298 K under a static pressure of 1 atmosphere, and is driven by a 1 MHz sound field of acoustic pressure amplitude 0.424 MPa. (a) The radius-time history, (b) the ratio of the temperature of the gas within the bubble to the initial value (298 K); (c) the ratio of the pressure of the gas within the bubble to the initial value; and (d) the ratio of the current number of moles of gas within the bubble to the initial number.

10 ***Figure 2*:** Modelling results on an Oxygen filled bubble incorporating mass flux across the bubble wall. The bubble is initially at rest in water at 298 K under a static pressure of 1 atmosphere, and is driven by a 1 MHz sound field of acoustic pressure amplitude 0.424 MPa. (a) The radius-time history, (b) the ratio of the temperature of the gas within the bubble to the initial value (298 K); (c) the ratio of the pressure of the gas within the bubble to the initial value; and (d) the ratio of the current number of moles of gas within the bubble to the initial number.

11 ***Figure 3:*** Modelling results on a Carbon Dioxide filled bubble incorporating mass flux across the bubble wall. The bubble is initially at rest in water at 298 K under a static pressure of 1 atmosphere, and is driven by a 1 MHz sound field of acoustic pressure amplitude 0.424 MPa. (a) The radius-time history, (b) the ratio of the temperature of the gas within the bubble to the initial value (298 K); (c) the ratio of the pressure of the gas within the bubble to the initial value; and (d) the ratio of the current number of moles of gas within the bubble to the initial number.

12 ***Figure 4*:** Modelling results on a Helium filled bubble with mass flux across the bubble wall forbidden. The bubble is initially at rest in water at 298 K under a static pressure of 1 atmosphere, and is driven by a 1 MHz sound field of acoustic pressure amplitude 0.424 MPa. (a) The radius-time history, (b) the ratio of the temperature of the gas within the bubble to the initial value (298 K); and (c) the ratio of the pressure of the gas within the bubble to the initial value.

13 ***Figure 5*:** Modelling results on an Oxygen filled bubble with mass flux across the bubble wall forbidden. The bubble is initially at rest in water at 298 K under a static pressure of 1 atmosphere, and is driven by a 1 MHz sound field of acoustic pressure amplitude 0.424 MPa. (a) The radius-time history, (b) the ratio of the temperature of the gas within the bubble to the initial value (298 K); and (c) the ratio of the pressure of the gas within the bubble to the initial value.

14 ***Figure 6*:** Modelling results on a Carbon Dioxide filled bubble with mass flux across the bubble wall forbidden. The bubble is initially at rest in water at 298 K under a static pressure of 1 atmosphere, and is driven by a 1 MHz sound field of acoustic pressure amplitude 0.424 MPa. (a) The radius-time history, (b) the ratio of the temperature of the gas within the bubble to the initial value (298 K); and (c) the ratio of the pressure of the gas within the bubble to the initial value.

15 ***Figure 7:*** Histograms of the largest peak temperatures attained during bubble collapses in the first fifty insonation cycles, as predicted by the Gilmore model which incorporates mass flux across the bubble wall, for an isolated bubble containing (a) helium, (b) oxygen, and (c) carbon dioxide. All other parameters are as for figure 1.

16 ***Figure 8:*** Histograms of the largest peak temperatures attained during bubble collapses in the first fifty insonation cycles, as predicted by the Gilmore model with mass flux across the bubble wall forbidden, for an isolated bubble containing (a) helium, (b) oxygen, and (c) carbon dioxide. All other parameters are as for figure 1.

17 ***Figure 9:*** The peak gas temperatures found in the modelling which exceed 960 K, the threshold temperature chosen to define inertial cavitation after the analysis of Flynn and Church (1988), as calculated by Holland and Apfel (1989). The 1550 K threshold chosen by Sponer (1990, 1991, Sponer et al., 1990) and the 5000 K threshold chosen by Holland and Apfel (1989) are also shown.

I. INTRODUCTION

Kondo (1994) has presented a scheme categorising the cavitational effects observed in a wide range of experiments with mon-, di-, and tri-atomic gases (Kondo et al. 1985, 1986, 1988, 1989a, 1989b, 1990; Kondo and Kano 1988). The effects include first free radical production, which is taken to indicative of the generation of high temperatures during collapse. Second, there are mechanical effects, including those associated with the collapse (hydrodynamic shear and the emission of shock waves into the liquid) and those associated rather with shear stresses brought on through microstreaming circulation. From these the type of cavitation, inertial or non-inertial, is inferred.

Certain features of the scheme (Table 1) are immediately explicable. The ratio of the specific heat of the gas at constant pressure (C_p) to its value at constant volume (C_v) is typified by the parameter γ, which is high for monatomic gases but lower for diatomic and triatomic gases (Table 2). It follows from the gas laws therefore that for a given compression ratio V_2/V_1, where V_2 is the final volume of the bubble and V_1 the initial size, that the final temperature T_2 will be greater the larger the value of γ. The law states that for a fixed mass of gas which behaves adiabatically, the pressure P is related to the volume V through

$$PV^{\gamma} = constant \tag{1}$$

Combining this with the ideal gas law, $PV \propto T$ for a fixed mass of gas, yields

$$TV^{\gamma-1} = constant \tag{2}$$

such that

$$\frac{T_2}{T_1} = \left(\frac{V_2}{V_1}\right)^{1-\gamma} \tag{3}$$

Therefore, for example, for a given adiabatic compression ratio of $V_2/V_1 = 0.1$, then for helium, oxygen, and carbon dioxide respectively the values of T_2/T_1 are 4.68, 2.49 and 2.00 respectively. That the final temperature in oxygen is only slightly greater than in carbon dioxide is not surprising, since their respective values of γ are 1.396 and 1.30, much less than that for a monatomic gas such as helium (where $\gamma = 1.667$). However this apparent similarity between the two gases is not reflected in the results shown in Table 1, where free radical production, the parameter which is assumed to be thermally-mediated, is similar for both helium and oxygen, but is not observed in carbon dioxide. The apparent discrepancy lies in the fact that the above calculation assumes identical compression ratios in fixed masses of gas, assumptions which are unlikely to hold true when the details of the cavitation dynamics are revealed. The purpose of this paper is to elucidate those details. Inertial cavitation is a threshold phenomenon, and the aim of the modelling is to indicate why in this sound field a typical population of bubbles containing carbon dioxide are sub-threshold, whilst those containing helium or oxygen will undergo inertial cavitation.

II. METHODS

The bubble oscillation simulations were performed by numerically solving the Gilmore-Akulichev model for bubble dynamics. The model seeks to solve the Gilmore equation of motion at discrete time intervals using a fourth order Runge-Kutta method. The time increment is calculated using a step-size control algorithm set to maintain a user-specified round-off error value. The equation of motion which is implemented is:

$$\frac{dU}{dt} = \frac{1}{R\left(1-\frac{U}{c_L}\right)}\left[\left(1+\frac{U}{c_L}\right)H - \frac{3U^2}{2}\left(1-\frac{U}{3c_L}\right)\right] + \frac{1}{c_L}\frac{dH}{dt} \tag{4}$$

where U is the radial velocity of the bubble wall, c_L is the local speed of sound calculated at the bubble wall, R is the instantaneous bubble radius and H is the enthalpy of the surrounding fluid. At each time step, the molar gas diffusion is calculated, the new equilibrium bubble radius found to reflect this gas transfer, and the temperature inside the bubble estimated. The model performs better than many of the others which are based on less stringent assumptions, in that it allows for the three methods of bubble damping. Acoustic radiation into the medium is incorporated through the provision of a variable speed of sound at the bubble wall, viscous damping is included when the pressure just outside the bubble wall is estimated, which in turn is required in the calculation of the local speed of sound and liquid enthalpy, and thermal losses are included in the choice of polytropic index. Bubble fragmentation and shape deviations from spherical, which may occur in practice, are not permitted in the model. The simulations were performed in Matlab, and took around 15 hours each to run. To more clearly show the effect of gas diffusion across the bubble boundary, the models were also solved for the cases when no mass flux is allowed.

In most of the experiments performed by Kondo and co-workers the bubbles were driven by a sound field with an intensity, I, of 6 W/cm^2, and is taken to be plane wave. Simple calculation gives an equivalent acoustic pressure amplitude of $p = \sqrt{(2\rho cI)} =$ 0.424 MPa. The choice of initial bubble size to be incorporated into the model can be decided through the requirement to study inertial cavitation. In a sound field of an amplitude which *exceeds* the threshold value, there exists a range of initial bubble sizes which will undergo inertial cavitation, and the greater the amplitude of insonation, the broader that range (Leighton, 1994). *At* the threshold acoustic pressure, only bubbles of one initial size will undergo inertial cavitation, and in a 1 MHz sound field those are bubbles with radii of initially ~ 0.6 μm (for air bubbles in water under 1 atmosphere static pressure), with the threshold peak negative pressure being ~ 0.3 MPa (Apfel and Holland, 1991). Since this investigation deals with the general case, it is more reasonable to chose a bubble size away from this optimum size: an initial radius of $R_0 =$ 5 μm was chosen.

III. RESULTS

Figures 1 to 3 show the results of modelling the response of a 5 μm bubble, initially at rest in water at 298 K under a static pressure of 1 atmosphere, to a 1 MHz sound field of acoustic pressure amplitude 0.424 MPa. In the results contained in figure 1 the bubble contains helium, in figure 2 oxygen, and figure 3 carbon dioxide. In each case the plot shows (a) the radius-time history, (b) the ratio of the temperature of the gas within the bubble to the initial value (298 K); (c) the ratio of the pressure of the gas within the bubble to the initial value; and (d) the ratio of the current number of moles of gas within the bubble to the initial number.

As expected, the diffusion of CO_2 is very great (number of moles of gas in bubble increases to about 150% of starting value after 50 cycles) compared with O_2 (increases to 102%) and He (101%). Therefore we might expect any effects due to gas diffusion to be great with CO_2, and much less with O_2 and He.

Figures 4 to 6 show the results of similar calculations, but for the situation when mass flux across the bubble wall is forbidden (clearly in each figure part (d) is not shown, being therefore constant at unity).

IV. DISCUSSION

There have been various ways proposed and used to characterise the threshold above which inertial cavitation is said to occur, and below which it said to be absent. Kondo takes free-radical production to be thermally mediated (which, whilst not universal, has certainly been the most popular view, the results of sonoluminescence from stable bubbles excepted - see Leighton 1994, Crum and Cordry 1994). The results may in the first instance be analysed by noting the temperature peaks which occur in the first fifty cycles of the oscillation. This is done in figure 7 for (a) helium, (b) oxygen, and (c) carbon dioxide when mass flux across the bubble wall is allowed, and in figure 8 for when it is forbidden. Simple first order examinations show the expected trend. The highest temperatures when gas flux is forbidden reflect the ratios estimated in the introduction for fixed masses of gas: $T_2/T_1 \sim 15$ (He; see figure 7a), ~ 8 (O_2; see figure 7b), and ~ 5.5 (CO_2; see figure 7c).

Comparing plots for 'with gas flux' (figure 7) and 'no gas flux' (figure 8) for each gas, there is, as expected, little change in the cases where the bubble contains helium (figures 7a and 8a) and oxygen (figure 7b and 8b). For CO_2 the histogram with gas flux (figure 7c) shows the higher maximum temperatures, though the mode has shifted *up* from a value of 2.5 (in figure 8c) to 4 (figure 7c). So the effect of gas flux is to make collapses more uniform, as would be expected: during the largest expansions, which would tend to generate the high collapse temperatures, the gas flux into the bubble is greatest, tending to cushion the subsequent collapse and reduce the maximum pressure attained.

Referring therefore to the thermal criterion for inertial cavitation, one important analysis (Apfel and Holland, 1991; Holland and Apfel, 1989) obtained an analytical

formulation for the inertial cavitation threshold based on the collapsing bubble achieving temperatures in excess of some chosen value. Holland and Apfel chose 5000 K, citing as a basis for this sonochemical results obtained using comparative rate thermometry performed by Suslick *et al.* (1986). However, after comparing their work with that of Flynn and Church (1988), they chose a different threshold. Flynn and Church employed the Gilmore-Akulichev model of bubble motion, much as is used in this paper, but to define the threshold condition pertaining to inertial cavitation, they calculated the acoustic sound pressure which would give rise to an expansion ratio $R_{max}/R_0 = 2$ (R_{max} being the maximum radius attained by the bubble, to which it has expanded from an initial radius R_0, and which it achieves just prior to the inertial collapse). The maximum temperature attained during the inertial collapse will depend on the expansion ratio R_{max}/R_0, and since they are not independent, Holland and Apfel adjusted their definition of inertial cavitation to occur when the bubble attained a temperature of 960 K, to allow comparison of their threshold with that of Flynn and Church. Though there are differences, agreement between the two sets of predictions (Holland and Apfel (1989), and Flynn and Church (1988)) is good for small nuclei and low frequencies. Sponer (1990, 1991; Sponer *et al.* 1990), in attempting to determine the thresholds for sonoluminescence, models the adiabatic collapse of an isolated gas bubble in a viscous compressible liquid, and sets the cavitation threshold to be the acoustic pressure required to attain a collapse temperature of 1550 K.

Clearly therefore there exists the idea that one approach to characterising the threshold for inertial cavitation might be to specify some maximum gas temperature attained during the course of the collapse, though a precise value of the critical gas temperature (if it exists) has not been settled. Even if it were, then the temperature required to cause thermal dissociation will depend on the species present. In addition free radicals may be generated through the passage of a shock wave through the gas, rather than be associated with the assumed spatially-uniform gas temperature distribution (Bradley, 1968; Vaughan and Leeman 1989). Even so it is useful to consider how the results displayed in figures 7 and 8 might be interpreted if a threshold gas temperature were assigned to the phenomenon.

Several facts are apparent. From Table 1, whilst oxygen bubbles lie above the threshold for free-radical production in Kondo's experiments, carbon dioxide bubbles lie below it. Mass flux across the bubble wall occurs significantly with carbon dioxide, but not with the other gases. The effect of this mass flux is to eliminate from the first fifty cycles those collapses which generate the highest temperatures. The maximum temperature recorded in the first fifty cycles, shown as the shaded item in figure 7c, corresponds to a temperature of 5.2×298 K $\approx$ 1550 K. If no mass flux were to have occurred, there would have been four collapses at temperatures in excess of this.

Bubbles containing the other gases included in Table 1 would similarly experience levels of mass flux commensurate with their solubilities (as shown in Table 2) during insonation, giving inertial cavitation or not, as indicated in Table 1. In the absence of inertial cavitation, the effects of microstreaming may be observed if the bubble if large enough: Large bubbles may appear through prolonged rectified diffusion in water saturated with CO_2 or N_2O, where the cushioning of the collapses which results from the mass flux prevents the highest-amplitude pulsations from causing bubble break-up before the bubbles attain a size large enough to generate significant microstreaming.

Whilst this is the case study of a single bubble size only, it is indicative that the combined effects of a smaller value of γ and significant flux of mass across the bubble wall combine to reduce the temperatures attained when carbon dioxide bubbles are insonated compared with those found with oxygen and helium. The experimental results (Table 1) indicate that the threshold for inertial cavitation occurs above those conditions generated by the insonation of carbon dioxide bubbles, but below those produced in bubbles of oxygen and helium. If free-radical production is assumed to be thermally-mediated, and if it is assumed that the signal-to-noise ratio is adequate to detect free radicals generated by a single collapse which exceeds the threshold, then the highest temperature attained during the collapse of carbon dioxide bubbles is less than the threshold, and the highest temperatures attained with the collapses of oxygen and helium bubbles are greater than the threshold. The models performed here, whilst limited to bubbles of initial radius 5 μm, can now be incorporated into this scheme for illustrative purposes. Figure 9 shows the modelled gas temperatures attained during those collapses which exceed 960 K, the threshold temperature chosen to define inertial cavitation after the analysis of Flynn and Church (1988), as calculated by Holland and Apfel (1989). The 1550 K threshold chosen by Sponer (1990, 1991, Sponer et al., 1990) and the 5000 K threshold chosen by Holland and Apfel (1989) are also shown. Since the carbon dioxide bubbles in Kondo's experiments were sub-threshold, but the oxygen and helium bubbles attained conditions which exceeded the threshold for inertial cavitation, the results from the 5 μm bubbles suggest that the 960 K threshold is too low (since all three gas bubble types exceed this), and that the 5000 K threshold is too high (since all three gas bubble types fail to achieve this threshold). The 1550 K threshold just satisfies the requirement that the carbon dioxide bubbles are sub-threshold, but the oxygen and helium bubbles achieve temperatures greater than threshold.

This analysis is by no means conclusive. Details of the size population of nuclei initially present in a sample are not available, and if they were would change during the experiment. The modelling of thermal losses by the Gilmore equation is limited. Some would contest that free radical production can be related to a threshold gas temperature: however the implications if it can must be explored given that this assumption is the basis for the 'mechanical index' (Apfel and Holland 1991) by which the likelihood of a system (e.g. a clinical ultrasound device) producing inertial cavitation is assessed.

V. CONCLUSIONS

The temperature attained during the collapses of bubbles in a sound field depend on numerous factors. In this study the effect of γ and mass flux across the bubble wall were studied. Carbon dioxide and oxygen has similar values of γ, both much less than that of helium; however the mass flux seen in carbon dioxide is many times greater than that seen in helium or oxygen. Since experimental studies indicate that in a similar sound field to that modelled here, carbon dioxide bubbles do not undergo inertial collapse but helium and oxygen bubbles do, this suggests that the mass flux seen with carbon dioxide is the important factor. For the bubbles modelled here (i.e. having initially a 5μm radius), the limited results suggest that of the three critical gas

temperatures proposed for the threshold for inertial cavitation, the closest is that of Sponer, at 1550 K.

VI. REFERENCES

Apfel RE, Holland CK. Gauging the likelihood of cavitation from short-pulse, low-duty cycle diagnostic ultrasound. *Ultrasound in Med. & Biol.* 1991; **17**: 179-185.

Bradley JN. *Shock waves in chemistry and physics.* Publ. Methuen & Co. 1968; pp. 246-263

Crum, LA, Cordry, S. Single-bubble sonoluminescence. in *Bubble Dynamics and Interface Phenomena* (FR Blake et al., eds.) Kluwer Academic Publishers, 1994. pp. 287-297.

Flynn HG, Church CC. Transient pulsations of small gas bubbles in water. *J Acoust Soc Am* 1988; **84**: 985-998

Holland CK, Apfel RE. An improved theory for the prediction of microcavitation thresholds. *IEEE transactions on ultrasonics, Ferroelectrics, and Frequency control* 1989; **36**: 204-208

Kondo, T; Arai, S; Kuwabara, M; Yoshii, G; Kano, E. Damage in DNA irradiated with 1.2 MHz ultrasound and its effect on template activity of DNA for RNA synthesis. *Radiat. Res.* 1985; **104**: 284-292

Kondo, T; Kuwabara, M; Sato, F; Kano E. Influence of dissolved gases on chemical and biological effects of ultrasound. *Ultrasound in Med. & Biol.* 1986; **12**: 151-155

Kondo, T; Kano, E. Effects of free radicals induced by ultrasonic cavitation on cell killing. *Int. J. Radiat. Biol.* 1988; **54**: 475-486

Kondo, T; Gamson, J; Mitchell, J.B; Riesz, P. Free radical formation and cell lysis induced by ultrasound in the presence of different rare gases. *Int. J. Radiat. Biol.* 1988; **54**: 955-962

Kondo, T; Fukushima, Y; Kon, H; Riesz, P. Effect of shear stress and free radicals induced by ultrasound on erythrocytes. *Arch. Biochem. Biophys.* 1989a; **269**: 381-389

Kondo, T; Krishna, C.M; Riesz, P. Sonolysis of concentrated aqueous solutions of nonvolatile solutes: Spin-trapping evidence for free radicals formed by pyrolysis. *Radiat. Res.* 1989b; **118**: 211-229

Kondo, T; Krishna, C.M; Riesz, P. Pyrolysis radicals formed by ultrasound in aqueous solutions of nucleotides: A spin trapping study. *Int. J. Radiat. Biol.* 1990; **57**: 23-33

Kondo, T. 1994. Personal communication.

Leighton, TG. 1994. *The Acoustic Bubble* (Academic P'ress, London). Section 4.3, section 5.2.

Sponer J, Davadorzh C, Mornstein V. The influence of viscosity on ultrasonic cavitation threshold for sonoluminescence at low megahertz region. *Studia Biohys* 1990; **137**: 81-89

Sponer J. Dependence of ultrasonic cavitation threshold on the ultrasonic frequency. *Czech J Phys B* 1990; **40**: 1123-1132

Sponer J. Theoretical estimation of the cavitation threshold for very short pulses of ultrasound. *Ultrasonics* 1991; **29**: 376-380

Suslick KS, Hammerton DA, Cline RE Jr. The sonochemical hot-spot. *J Am Chem Soc* 1986; **108**: 5641-5642

Vaughan, PW, Leeman, S. Acoustic cavitation revisited. *Acustica* 1989; **69**: 109-119

TABLES

	Gases	Type of Cavitation	Free Radicals [1]	Mechanical Effects [2]
Monatomic [3]	Xe	Inertial	+++++	+
	Kr	Inertial	++++	+
	Ar	Inertial	+++	+ Hydrodynamic shear
	Ne	Inertial	++	+ and/or shock wave
	He	Inertial	+	+ due to collapse
Diatomic	O_2	Inertial	+	+ Same as above
	N_2	Inertial	+	+
Triatomic	N_2O	Non-inertial	–	+/– Shear stress due to
	CO_2	Non-inertial	–	+/– micro streaming [4]

1) Free radical formation is temperature (of cavitation bubble) dependent phenomena.
2) Cell lysis due to mechanical effect is temperature independent phenomena.
3) Temperature in the presence of monatomic gases depend on thermal conductivity. Temperature in the presence of mon-, di-, and tri-atomic gases depend on γ value.
4) Positive or negative depends on size of resonant bubbles (i.e. frequency dependent).

Table 1: Summary of the experimental findings of Kondo and co-workers (Kondo 1994, personal communication). The symbol '+' indicates a positive finding, the more symbols the greater the magnitude of the effect observed. The symbol '-' indicates that the effect was not observed. The symbol '+/-' indicates a marginal effect.

	He	O_2	CO_2
C_p/C_v	1.67	1.40	1.28
Diffusivity @ 25 °C [m^2/s]	6.28×10^{-9}	2.1×10^{-9}	1.92×10^{-9}
Solubility in water @ 25 °C	0.0087	0.029	0.772

Table 2: Data for calculations employed in the Gilmore model, and for other relevant gases.

FIGURES

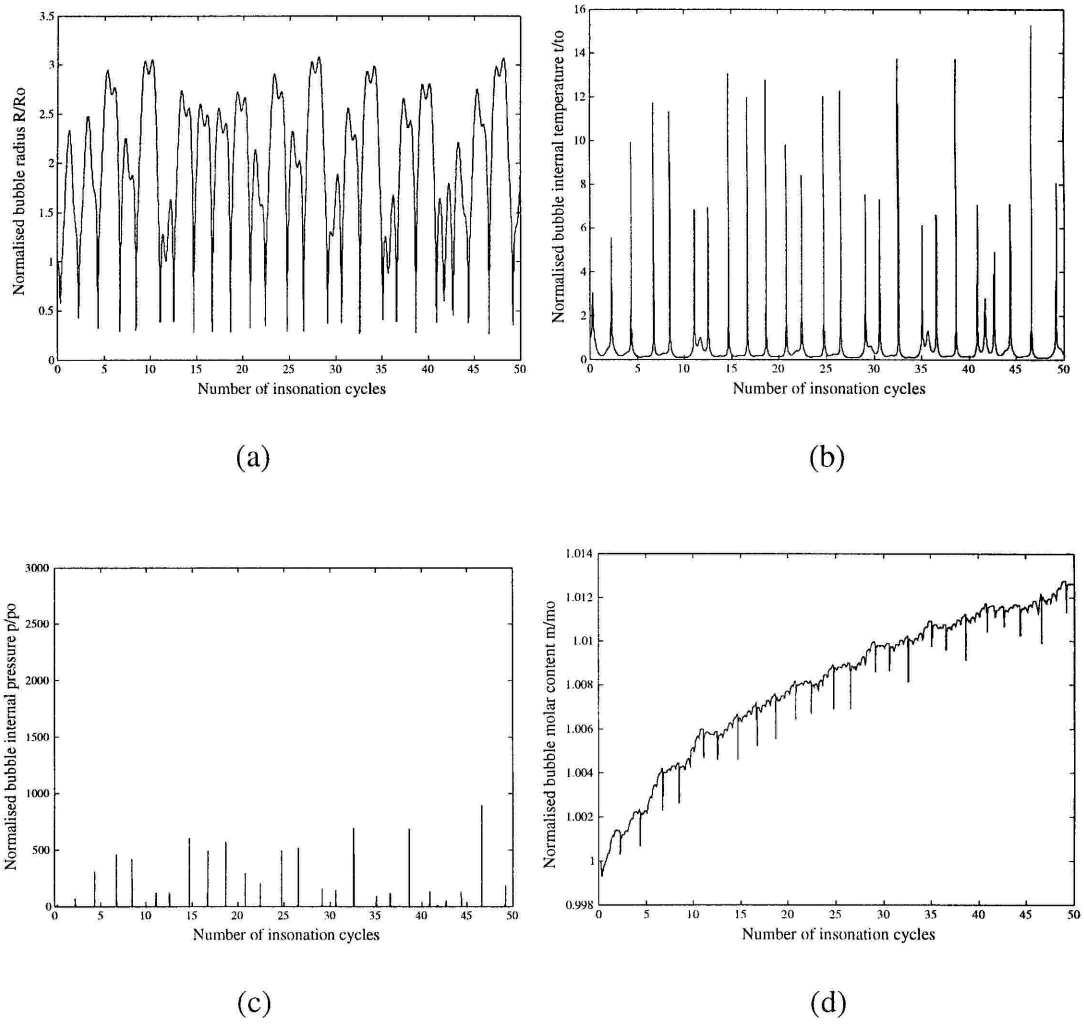

***Figure 1*:** Modelling results on a Helium filled bubble incorporating mass flux across the bubble wall. The bubble is initially at rest in water at 298 K under a static pressure of 1 atmosphere, and is driven by a 1 MHz sound field of acoustic pressure amplitude 0.424 MPa. (a) The radius-time history, (b) the ratio of the temperature of the gas within the bubble to the initial value (298 K); (c) the ratio of the pressure of the gas within the bubble to the initial value; and (d) the ratio of the current number of moles of gas within the bubble to the initial number.

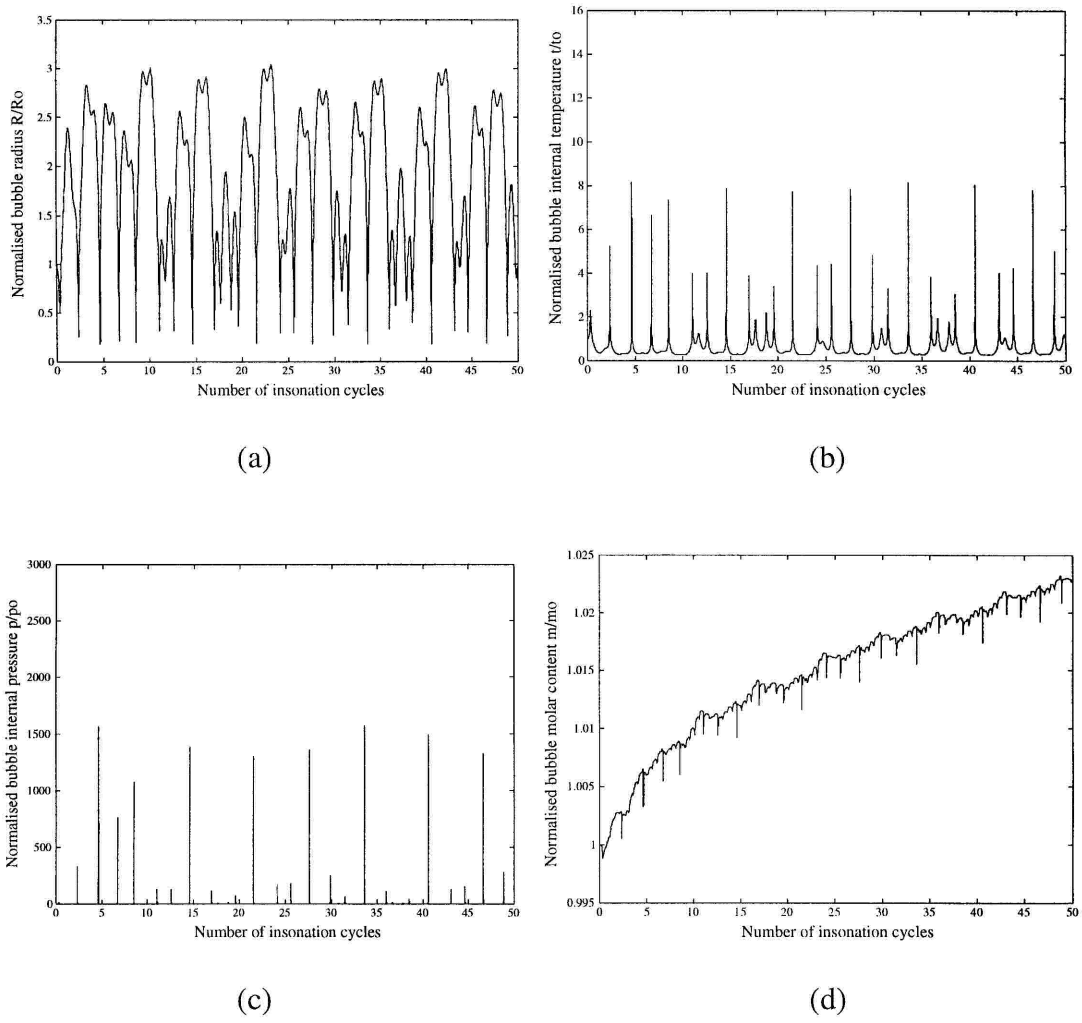

***Figure 2*:** Modelling results on an Oxygen filled bubble incorporating mass flux across the bubble wall. The bubble is initially at rest in water at 298 K under a static pressure of 1 atmosphere, and is driven by a 1 MHz sound field of acoustic pressure amplitude 0.424 MPa. (a) The radius-time history, (b) the ratio of the temperature of the gas within the bubble to the initial value (298 K); (c) the ratio of the pressure of the gas within the bubble to the initial value; and (d) the ratio of the current number of moles of gas within the bubble to the initial number.

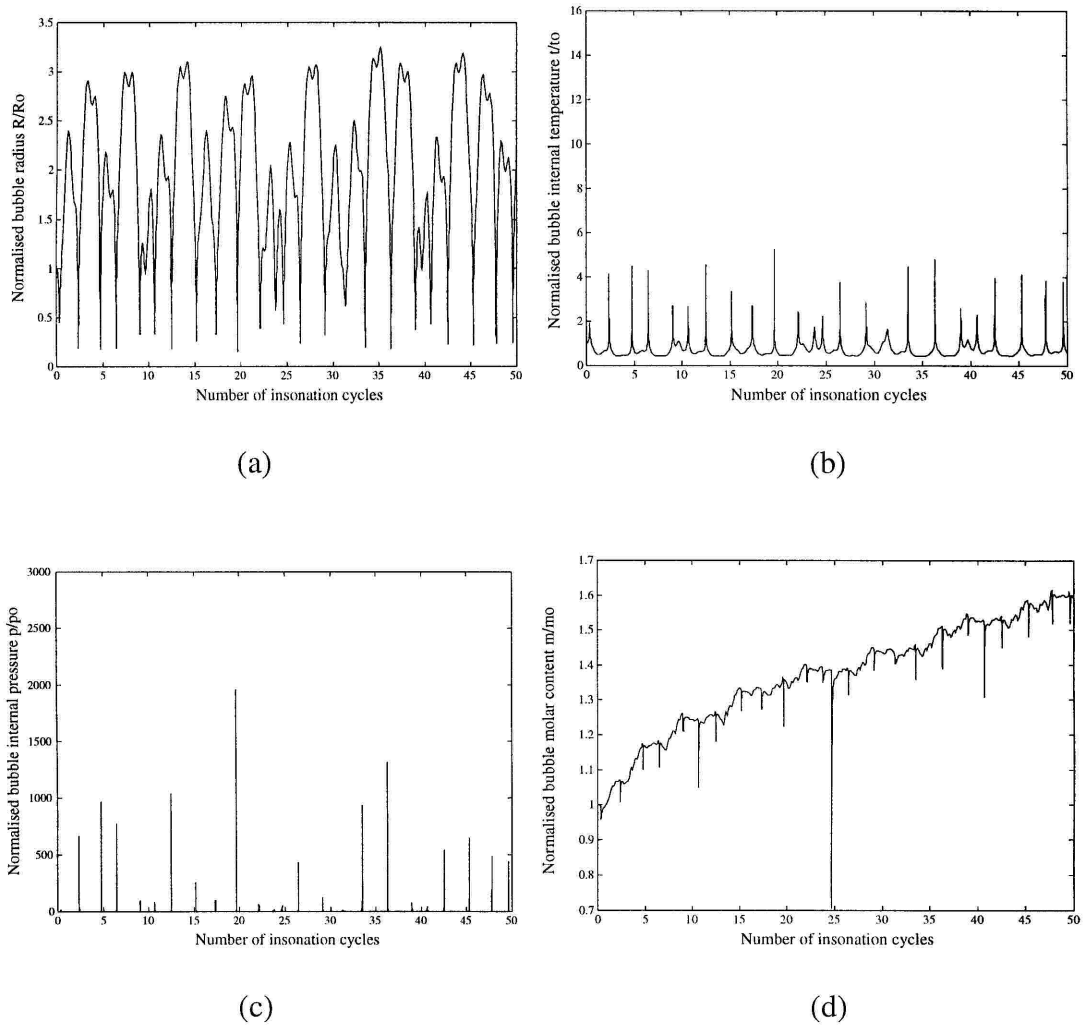

Figure 3: Modelling results on a Carbon Dioxide filled bubble incorporating mass flux across the bubble wall. The bubble is initially at rest in water at 298 K under a static pressure of 1 atmosphere, and is driven by a 1 MHz sound field of acoustic pressure amplitude 0.424 MPa. (a) The radius-time history, (b) the ratio of the temperature of the gas within the bubble to the initial value (298 K); (c) the ratio of the pressure of the gas within the bubble to the initial value; and (d) the ratio of the current number of moles of gas within the bubble to the initial number.

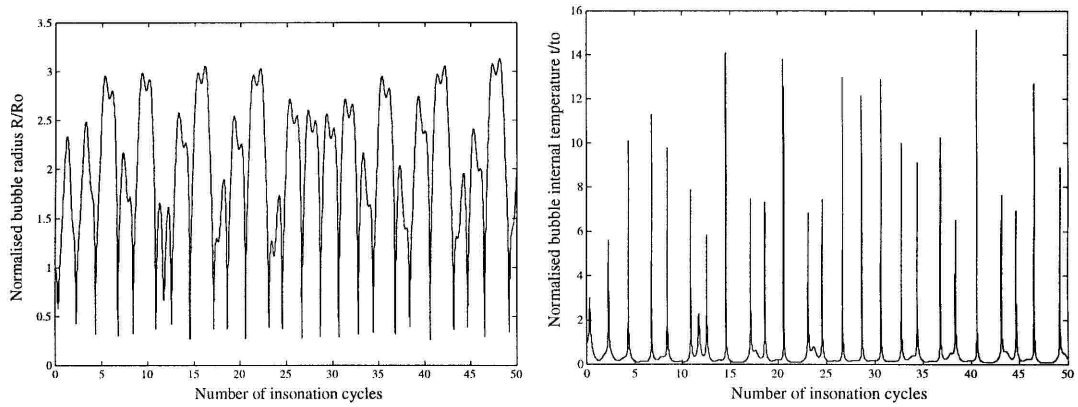

(a) (b)

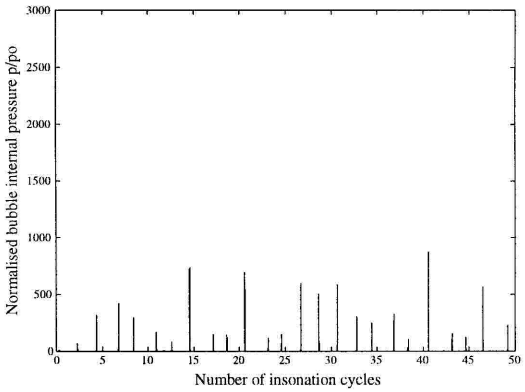

(c)

***Figure 4*:** Modelling results on a Helium filled bubble with mass flux across the bubble wall forbidden. The bubble is initially at rest in water at 298 K under a static pressure of 1 atmosphere, and is driven by a 1 MHz sound field of acoustic pressure amplitude 0.424 MPa. (a) The radius-time history, (b) the ratio of the temperature of the gas within the bubble to the initial value (298 K); and (c) the ratio of the pressure of the gas within the bubble to the initial value.

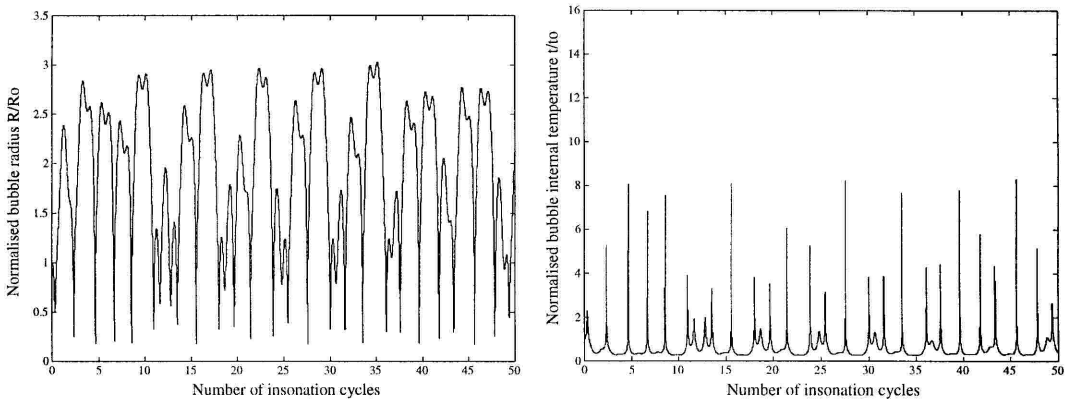

(a) (b)

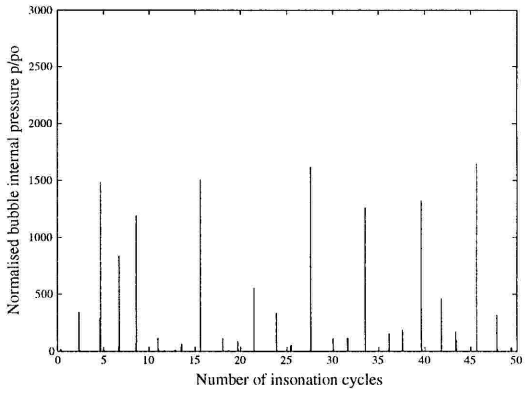

(c)

***Figure 5*:** Modelling results on an Oxygen filled bubble with mass flux across the bubble wall forbidden. The bubble is initially at rest in water at 298 K under a static pressure of 1 atmosphere, and is driven by a 1 MHz sound field of acoustic pressure amplitude 0.424 MPa. (a) The radius-time history, (b) the ratio of the temperature of the gas within the bubble to the initial value (298 K); and (c) the ratio of the pressure of the gas within the bubble to the initial value.

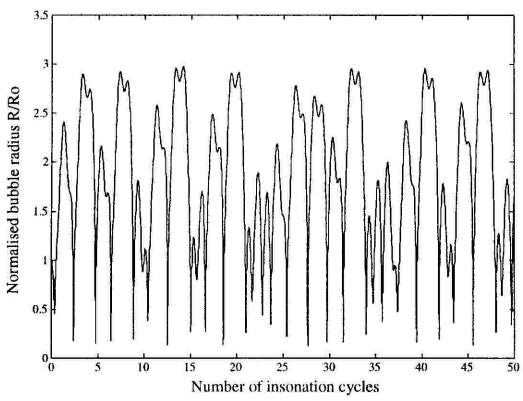

(a)

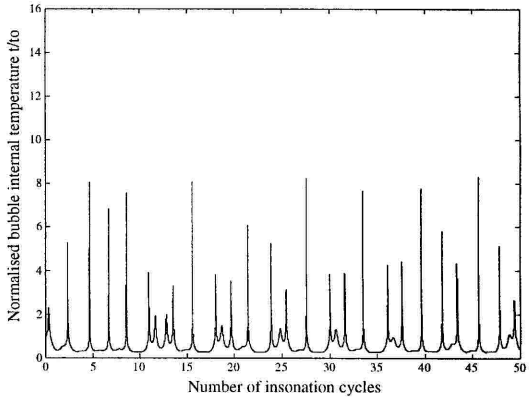

(b)

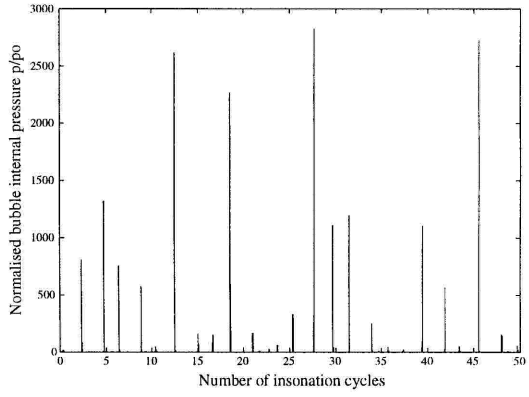

(c)

***Figure 6*:** Modelling results on a Carbon Dioxide filled bubble with mass flux across the bubble wall forbidden. The bubble is initially at rest in water at 298 K under a static pressure of 1 atmosphere, and is driven by a 1 MHz sound field of acoustic pressure amplitude 0.424 MPa. (a) The radius-time history, (b) the ratio of the temperature of the gas within the bubble to the initial value (298 K); and (c) the ratio of the pressure of the gas within the bubble to the initial value.

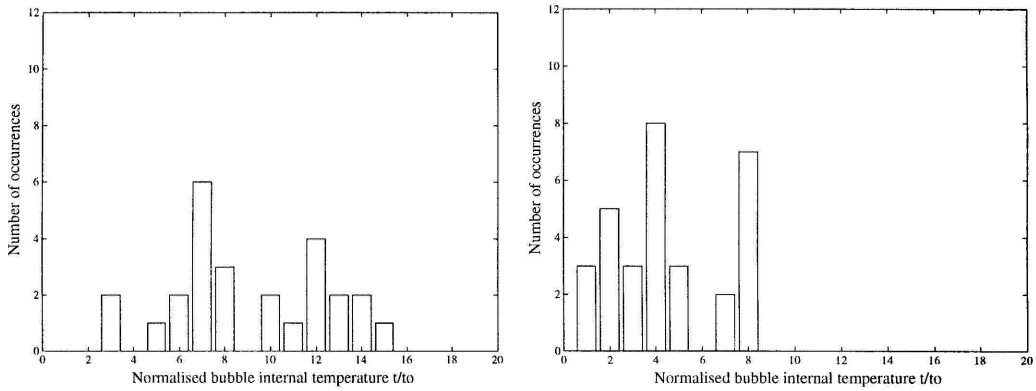

(a) (b)

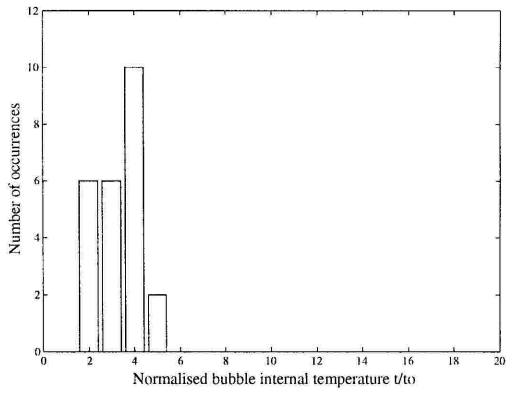

(c)

Figure 7: Histograms of the largest peak temperatures attained during bubble collapses in the first fifty insonation cycles, as predicted by the Gilmore model which incorporates mass flux across the bubble wall, for an isolated bubble containing (a) helium, (b) oxygen, and (c) carbon dioxide. All other parameters are as for figure 1.

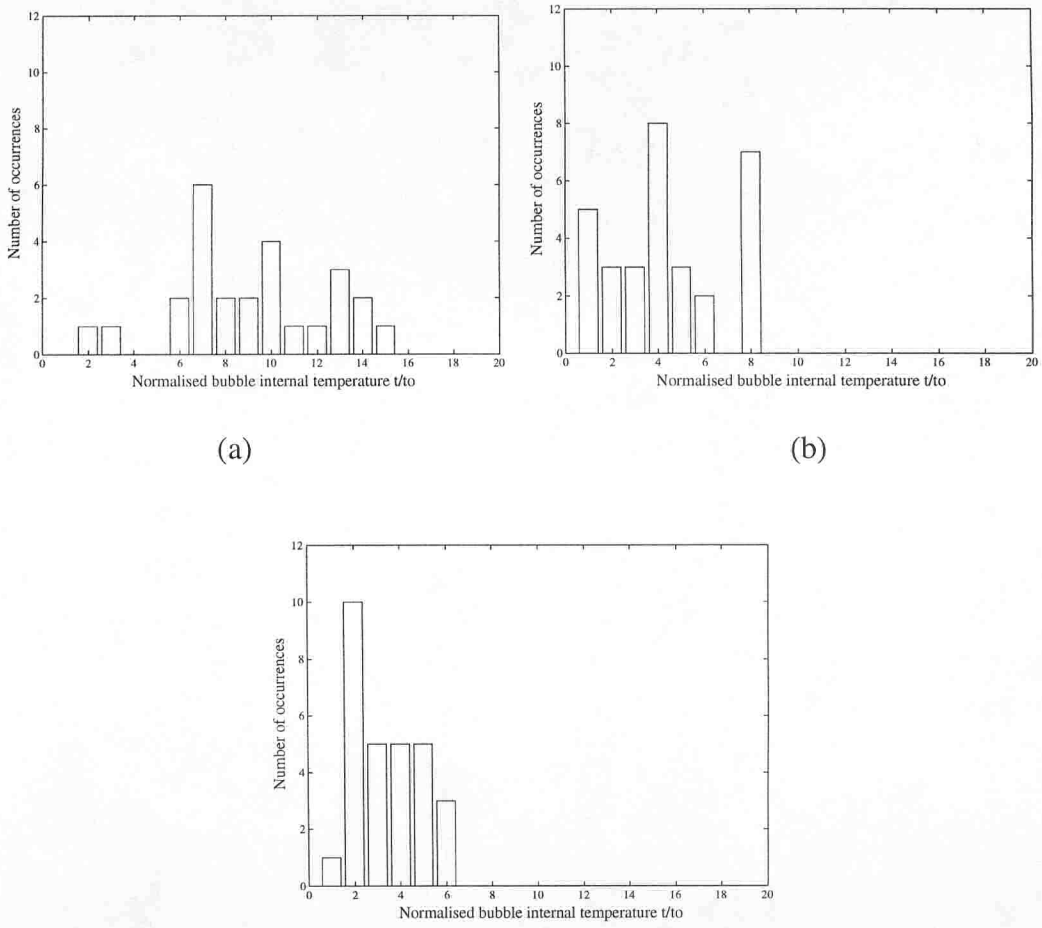

Figure 8: Histograms of the largest peak temperatures attained during bubble collapses in the first fifty insonation cycles, as predicted by the Gilmore model with mass flux across the bubble wall forbidden, for an isolated bubble containing (a) helium, (b) oxygen, and (c) carbon dioxide. All other parameters are as for figure 1.

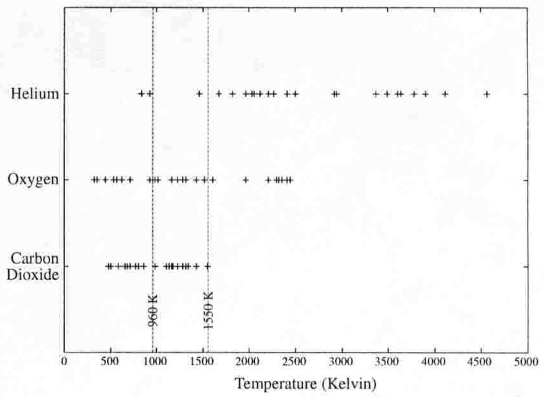

Figure 9: The peak gas temperatures found in the modelling which exceed 960 K, the threshold temperature chosen to define inertial cavitation after the analysis of Flynn and Church (1988), as calculated by Holland and Apfel (1989). The 1550 K threshold chosen by Sponer (1990, 1991, Sponer et al., 1990) and the 5000 K threshold chosen by Holland and Apfel (1989) are also shown.